

Large Scale Structure

Jaan Einasto

Tartu Observatory, EE-61602 Toravere, Estonia

Abstract

I give a review of catalogues of galaxies, clusters of galaxies and superclusters { sources of information to study the large{scale structure of the Universe. Thereafter I shall discuss the power spectrum of density perturbations, and the correlation function { principal description functions which characterize the large{scale structure. I shall pay special attention to the geometric interpretation of these functions, i.e. to the way in which the various properties of the distribution of galaxies in systems and systems themselves are reflected in these functions. Finally, I discuss cosmological parameters which characterize general properties of the Universe { the Hubble constant, densities of various populations of the Universe, and parameters of the power spectrum of galaxies and matter.

1 Introduction

In this review I shall accept certain paradigms on the structure of the Universe. Paradigms on the structure of the Universe have evolved considerably during the last hundred years. This process is continuing until the present time, and changes occur quite often, so it is important that we clearly state the present paradigms. I shall use the term "Universe" for the real world around us, and the term "universe" for a model of the Universe (say Friedmann{universe). Our accepted paradigms are:

The Universe evolves from an explosive event termed "Big Bang", through the inflation, the radiation{domination era to the matter{domination era; probably we live now in the next era where the dominating constituent of the Universe is dark energy.

The principal force driving the cosmological evolution is gravity.

Density perturbations grow from small random fluctuations generated during the inflation; perturbations have Gaussian distribution.

The main constituents of the Universe are: baryonic matter (stars and planets, hot and cold gas, and primordial gas in voids), dark matter, either cold (CDM) or hot (HDM), and dark (vacuum) energy.

The Universe is flat if the total mean density of all its populations is equal to the critical density.

There exist a number of excellent reviews on the subject "Large-scale structure of the Universe", the most recent one with references to earlier work is the talk by Guzzo [29] in the 19th Texas Symposium. The term "Large-scale structure of the Universe" itself originated in the contemporary meaning as the title of an IAU Symposium [33], where the presence of filamentary distribution of galaxies and clusters with large empty voids between them was first reported. In this review I use the experience collected at Tartu Observatory during the last 25-30 years of the study of the Universe. I shall pay attention to cosmographic aspects of the problem, in particular to the geometrical and physical interpretation of descriptive functions. Also I try to show how advances in observational cosmology have changed our theoretical understanding of the formation and evolution of the structure of the Universe.

2 Catalogues of galaxies, clusters and superclusters

Our understanding of the structure of the Universe is based on the distribution of galaxies. Until the mid-1970s the number of galaxies with known distances (redshifts) was very small, thus conclusions on the structure were based on counts of galaxies. The largest of such counts was compiled in Lick Observatory by Shane & Virtanen [51]. This catalogue was analyzed by Seldner et al. [49] and played a crucial role in the development of the hierarchical clustering scenario of structure formation by Peebles [42].

A big step in the study of the clustering of galaxies and clusters of galaxies was made by visual inspection of the Palomar Observatory Sky Survey plates with the aim to produce catalogues of galaxies and clusters of galaxies. The first of these catalogues was prepared by Abell [1] for clusters of galaxies. This catalogue covers the sky north of declination $\delta = 27^\circ$. Abell, Corwin & Olowin [2] extended the cluster catalogue to the southern sky. Both these catalogues together contain 4074 clusters. A much larger catalogue was compiled by Zwicky et al. [63]; in this catalogue all galaxies brighter than photographic magnitude $m_{ph} < 15.7$ as well as clusters of galaxies north of declination $\delta = 25^\circ$ are listed. Abell and Zwicky used rather different definitions of clusters. Abell clusters contain at least 30 galaxies in a magnitude interval of $m = 2$, starting from the third brightest galaxy, and located within a radius of $1.5 h^{-1} \text{ Mpc}$ (we use in this paper the Hubble constant in units $H_0 = 100 h \text{ km s}^{-1} \text{ Mpc}^{-1}$). Distances of clusters were estimated on the basis of the brightness of the 10th brightest galaxy. Clusters were divided to richness and distance classes. Zwicky used a more relaxed cluster definition, with at least 50 galaxies in a magnitude interval of $m = 3$, starting from the brightest galaxy, located within

a contour where the surface density of galaxies exceeded a certain threshold. Due to these differences some Zwicky clusters are actually central parts of superclusters which contain several Abell clusters and groups of galaxies (an example is the Perseus cluster). Since the definition of clusters in the Abell catalogue is more exact, this catalogue has served for a large number of studies of the structure of the Universe. On the other hand, the Zwicky catalogue of galaxies was the basic source of targets for redshift determinations.

An early catalogue of bright galaxies was compiled by Shapley & Ames [53]. Sandage & Tammann [48] published a revised version of this catalogue; it contains data on galaxies brighter than 13.5 magnitude, including redshifts. This catalogue, and the compilation of all available data on bright galaxies by de Vaucouleurs, de Vaucouleurs, & Corwin [18] were the sources of distances which allowed to obtain the first 3-dimensional distributions of galaxies. Much more detailed information on the spatial distribution of galaxies was obtained on the basis of redshifts, measured at the Harvard Center for Astrophysics (CfA) for all Zwicky galaxies brighter than $m_{ph} = 14.5$. Later this survey was extended to galaxies brighter than $m_{ph} = 15.5$ (the second CfA catalogue), and to galaxies of the southern sky (Southern Sky Redshift Survey) [14].

These early redshift compilations made it possible to discover the filamentary distribution of galaxies and clusters forming huge superclusters, as well as the absence of galaxies between them. These results were first reported in the IAU Symposium on Large Scale Structure of the Universe [31,55,57,58] and demonstrated that the pancake scenario of structure formation by Zeldovich [60,61] fits observations better than the hierarchical clustering scenario. More detailed studies of the structure formation by numerical simulations showed that the original pancake scenario by Zeldovich also has weak points { there is no fine structure in large voids between superclusters observed in the real Universe [62] and the structure forms too late [16], thus a new scenario of structure formation was suggested based on the dominating role of the cold dark matter in structure evolution [5]. In a sense the new scenario is a hybrid between the original Peebles and Zeldovich scenarios: structure forms by hierarchical clustering of small structures within large filamentary structures { superclusters.

The next big step in the study of the large scale distribution of galaxies was made on the basis of the catalogue of galaxies formed on the basis of digitized images of the ESO Sky Survey plates using the Automated Plate Measuring (APM) Facility [36,37]. The APM galaxy catalogue covers 185 ESO fields, is complete up to magnitude $b_j = 20.5$, and was the basis for a catalogue of clusters prepared by Dalton et al. [15]. The analysis of the APM galaxy sample showed that properties of the distribution of galaxies differ from the standard CDM model which assumed that the density of matter is equal to the critical density. A low density model with cosmological term (dark energy) fits the

data better [19].

The modern era of galaxy redshift catalogues started with the Las Campanas Redshift Survey (LCRS). Here, for the first time, multi-object spectrographs were used to measure simultaneously redshifts of 50–120 galaxies [52]. The LCRS covers 6 slices of size 1.5×80 degrees, the total number of galaxies with redshifts is 26,000, and the limiting magnitude is $b_j = 18.8$. Presently several very large programs are under way to investigate the distribution of galaxies in a much larger volume. The largest project is the Sloan Digital Sky Survey (SDSS), a cooperative effort of several North American institutions with participants from Japan [34]. This survey covers the whole northern sky and a strip in the southern sky. The sky is first imaged in five photometric bands to a limiting magnitude about 23 (the limit varies with spectral bands), thereafter redshifts are measured for all galaxies up to a magnitude 18, and active galactic nuclei (AGN) up to 19; additionally a volume-limited sample of redshifts of bright elliptical galaxies is formed. The total number of galaxies with measured redshifts will probably exceed one million. Another large redshift survey uses the 2-degree Field [35] spectrograph of the Anglo-Australian Telescope. This survey is based on the APM galaxy catalogue and covers two large areas of size 75×12.5 and 65×7.5 with limiting magnitude $b_j = 19.5$. The goal is to measure about 250,000 redshifts. It is expected that new redshift surveys give us the possibility to investigate the detailed structure of the Universe up to a distance of $2000 h^{-1} \text{ Mpc}$.

The largest systems of galaxies are superclusters, which are defined as the largest systems of galaxies and clusters still isolated from each other. Catalogues of superclusters have been constructed using Abell clusters of galaxies. The latest compilation by Einasto et al. [26] contains 220 superclusters with at least two member clusters.

3 Distribution of galaxies and clusters

In Figure 1 I show the distribution of galaxies of various luminosity in a volume-limited sample through the Virgo, Coma and Hercules superclusters. We use supergalactic coordinates Y and Z in km/s , respectively, in a sheet $0 < X < 10 h^{-1} \text{ Mpc}$. Bright galaxies ($M_B < -20.3$) are plotted as red dots, galaxies $-20.3 < M_B < -19.7$ as black dots, galaxies $-19.7 < M_B < -18.8$ as open blue circles, galaxies $-18.8 < M_B < -18.0$ as green circles (absolute magnitudes correspond to Hubble parameter $h = 1$). High-density regions are the Local, the Coma and the Hercules superclusters in the lower left, lower right and upper right corners, respectively. The long chain of galaxies between Coma and Hercules superclusters is called the Great Wall. Actually it is a filament. For comparison, the distribution of particles in a 2-dimensional sim-

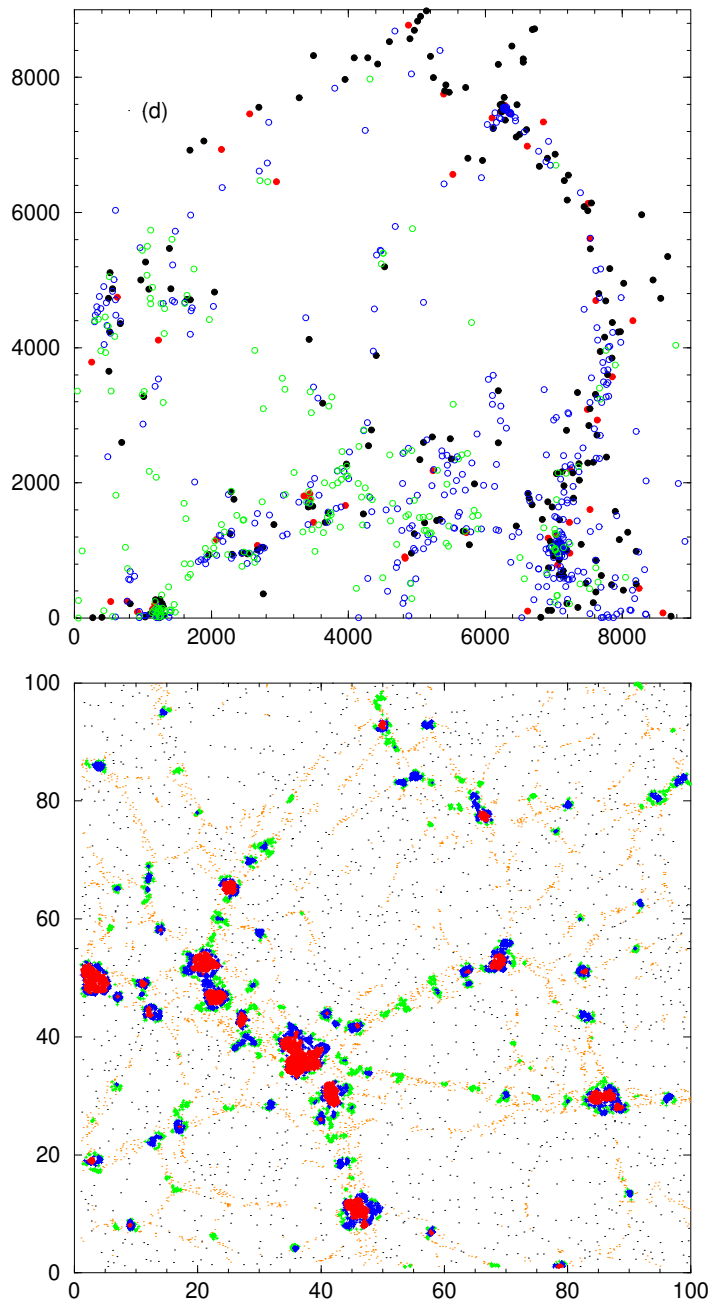


Fig. 1. The distribution of galaxies (upper panel), and particles in a 2-D simulation (lower panel). For explanations see text.

ulation is also plotted in a box of side-length $100 h^{-1} \text{ Mpc}$. Different colors indicate the density value of the particle environment. Particles in voids (density $\% < 1$) are shown as black dots; particles in the density interval $1\% < 5\%$ form filaments of galaxies (orange dots); particles with densities $5\% < 10\%$ (green dots) form groups of galaxies; particles with $10\% < 20\%$ (blue dots) form clusters; and particles with $\% \geq 20$ (red dots) are in very rich clusters. Densities are expressed in units of the mean density in the simulation; they are calculated using a smoothing length of $1 h^{-1} \text{ Mpc}$. Three-dimensional simulations have similar behaviour. This Figure emphasizes that particles in

high-density regions simulate matter associated with galaxies, and that the density of the particle environment defines the type of the structure. In both Figures we see the concentration of galaxies or particles to clusters and filaments, and the presence of large under-dense regions. There exists, however, one striking difference between the distribution of galaxies and simulated particles { there is a population of smoothly distributed particles in low-density regions in simulations, whereas in the real Universe voids are completely empty of any visible matter. This difference is due to differences of the evolution of matter in under- and over-dense regions.

Zeldovich [60] and Einasto, Jeeveer & Saar [24] have shown that the density evolution of matter due to gravitational instability is different in over- and under-dense regions. The evolution follows approximately the law

$$D_c(t) = \frac{1}{1 - d_0(t-t_0)}; \quad (1)$$

where d_0 is a parameter depending on the amplitude of the density fluctuations. In over-dense regions $d_0 > 0$, and the density increases until the matter collapses and forms pancake or filamentary systems [6] at a time t_0 ; thus the formula can be applied only for $t > t_0$. In under-dense regions we have $d_0 < 0$ and the density decreases, but never reaches zero (see Figure 2). In other words, there is always some dark matter in under-dense regions. At the time when over-dense regions collapse the density in under-dense regions is half of the original (mean) density. In order to form a galaxy the density of matter in a given region must exceed a certain critical value [44], thus galaxies cannot form in under-dense regions. They form only after the matter has flown to over-dense regions: filaments, sheets, or clusters; here the formation occurs in situ.

Consider the distribution of matter as a superposition of several sinusoidal waves of amplitude a_i and period p_i around the mean density D_m

$$D(r) = D_m + \sum_i a_i \sin(2\pi r/p_i); \quad (2)$$

Gravitational instability determines the evolution of these density perturbations: large high over-dense regions become superclusters; weakly over-dense regions become small filaments of galaxies and groups; under-dense regions become voids, see Figure 2. The fine structure of superclusters is defined by perturbations of medium wavelength, the structure of clusters by small-scale perturbations.

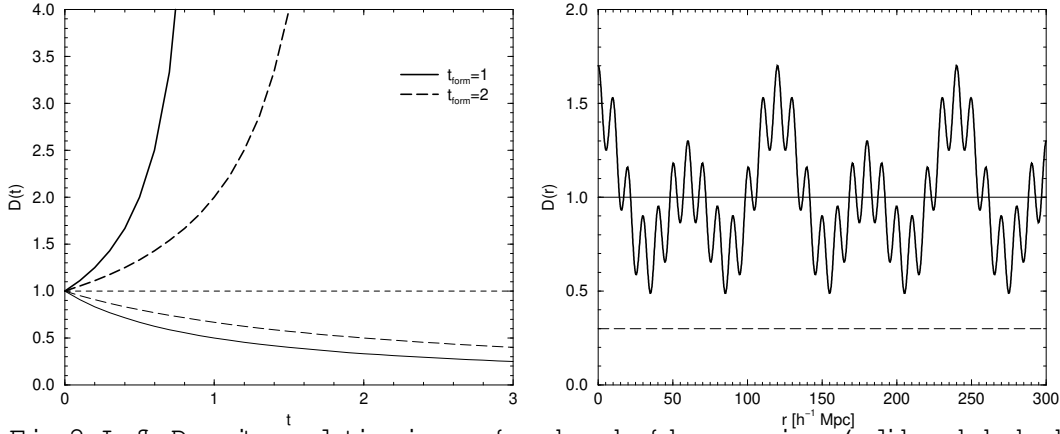


Fig. 2. Left: Density evolution in over- and under-dense regions (solid and dashed lines, respectively) for two epochs of caustics formation. Right: Density perturbations of various wavelengths. Under-dense regions ($D < 1$) become voids; strongly over-dense regions ($D > 1.3$) { superclusters (cluster chains); moderately over-dense regions ($1 < D < 1.3$) { filaments of groups and galaxies.

4 Description functions

Principal description functions that characterize the present large-scale structure of the Universe are the power spectrum of matter and galaxies, the correlation function of galaxies and clusters, the cluster mass distribution, the void probability function (VPF), and functions based on the clustering of galaxies and clusters { the multiplicity function, and the percolation function. The structure of the early Universe can be described by the angular spectrum of the Cosmic Microwave Background (CMB). Here we discuss in more detail properties of the power spectrum and correlation function, and their dependence on geometrical properties of the distribution of galaxies and clusters.

4.1 Power spectrum

The power spectrum describes the fluctuating density field $\delta(x)$ through its Fourier components δ_k

$$P(k) = \langle \delta_k \delta_k^* \rangle \quad (3)$$

Here k is the wavenumber in units of $h \text{ Mpc}^{-1}$. The power spectrum can be characterized by the power index on large scales, n , and by its amplitude on certain characteristic scales. For the last purpose usually very large scales ($> 1000 h^{-1} \text{ Mpc}$) are used, where the amplitude is fixed by CMB observations by the COBE satellite [10], and scales where the power spectrum becomes non-linear, $r < 8 h^{-1} \text{ Mpc}$. The amplitude of the power spectrum on this

scale can be expressed through the δ_8 parameter { which denotes the rms density fluctuations within a sphere of radius $8 h^{-1} Mpc$. It can be calculated by integrating the power spectrum of matter.

The comparison of the distribution of real galaxies and particles in simulations has shown that there are no luminous galaxies in voids; here the matter has remained in its primordial dark form. Now we consider the influence of the presence of dark matter in voids on the power spectrum of the clustered matter associated with galaxies. Low-density matter in voids forms a smooth background of almost constant density. The density contrast of matter $\delta(x)$ can be expressed as $\delta(x) = (D(x) - D_m) / D_m$, where $D(x)$ is the density at location x , and D_m is the mean density of matter averaged over the whole space under study. If we exclude from the sample of all particles a population of approximately constant density (void particles, see horizontal line in the right panel of Figure 2), but preserve all particles in high-density regions, then the amplitudes of absolute density fluctuations remain the same (as they are determined essentially by particles in high-density regions), but the amplitudes of relative fluctuations with respect to the mean density increase by a factor which is determined by the ratio of mean densities, i.e. by the fraction of matter in the new density field with respect to the previous one

$$\delta(x) = \frac{D(x) - D_c}{D_c} \frac{D_c}{D_m}; \quad (4)$$

here $D_c / D_m = F_c$ is the fraction of matter in the clustered (galaxy) population. A similar formula holds for the density contrast in Fourier space, and we obtain the relation between power spectra of matter and the clustered population

$$P_m(k) = F_c^2 P_c(k); \quad (5)$$

We define the biasing parameter of galaxies (actually of all clustered matter associated with galaxies) relative to matter through the ratio of power spectra of galaxies and matter. Both spectra are functions of the wavenumber k , thus the biasing parameter is a function of k . Numerical simulations by Einasto et al. [23] show that in the linear regime of the structure evolution the biasing parameter is practically constant for wavenumbers smaller than $k = 0.8 h Mpc^{-1}$ (scales larger than about $8 h^{-1} Mpc$). Its value found from simulations is very close to the expected value calculated from Equation (5). We come to the conclusion that the biasing parameter is determined by the fraction of matter in the clustered population

$$b_c = 1 = F_c; \quad (6)$$

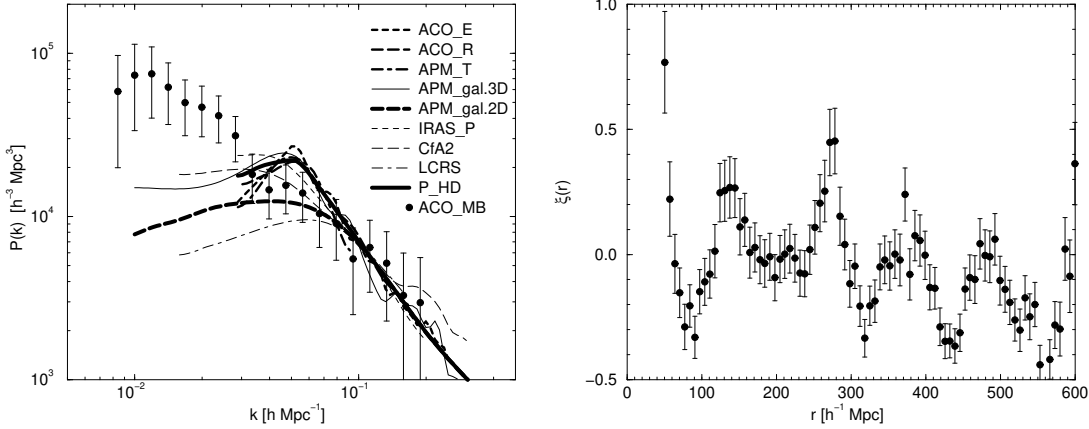


Fig. 3. Left: power spectra of galaxies and clusters of galaxies normalized to the amplitude of the 2-D APM galaxy power spectrum. For clarity error bars are not indicated and spectra are shown as smooth curves rather than discrete data points. Bold lines show spectra for clusters data. Points with error bars show the spectrum of Abell clusters by Miller & Batukhi [38] adjusted to the galaxy spectrum amplitude by a relative bias factor $b = 3.2$. Right: correlation function of Abell clusters located in superclusters with at least 8 clusters [20].

A summary of recent observational data on power spectra of galaxies and clusters of galaxies of various type is shown in the left panel of Figure 3, according to a compilation by Einasto et al. [22]. Galaxy and cluster spectra are adjusted in amplitude to reduce them to the power spectrum of APM galaxies. We assume that the amplitude of the power spectrum of APM galaxies represents well the amplitude of the whole clustered (galaxy) population. On large scales we use a recent determination [38] on the basis of Abell clusters of richness class 1 and higher.

4.2 Correlation function

The two-point correlation function $\xi(r)$ is defined as the excess over Poisson of the joint probability of finding objects in two volume elements separated by r and averaged over a very large volume [42]. We shall use the term "correlation function" for its estimate, determined in a limited volume, and calculate it using the formula:

$$\xi(r) = \frac{\langle D(r) \rangle - n^2}{n^2} \quad (7)$$

where $\langle D(r) \rangle$ is the number of pairs of galaxies (or clusters of galaxies) in the range of distances $r \pm dr/2$, dr is the bin size, $\langle R(r) \rangle$ is the respective number of pairs in a Poisson sample of points, n and n_R are the mean number densities of clusters in respective samples, and brackets $\langle \cdot \rangle$ denote the en-

semble average. The summation is over the whole volume under study, and it is assumed that the galaxy and Poisson samples have identical shape, volume and selection function.

Both the correlation function and the power spectrum characterise the distribution of galaxies, clusters and superclusters. In an ideal case in the absence of errors, and if both functions are determined in the whole space, they form a mutual pair of Fourier transformations:

$$\xi(r) = \frac{1}{2\pi^2} \int_0^\infty P(k) k^2 \frac{\sin kr}{kr} dk; \quad (8)$$

$$P(k) = 4\pi \int_0^\infty \xi(r) r^2 \frac{\sin kr}{kr} dr; \quad (9)$$

These formulae are useful when studying theoretical models or results of numerical simulations. For real samples they are of less use since observational errors and selection effects influence these functions in a different way. Also they reflect the spatial distribution of objects differently, thus they complement each other.

There exists a large body of studies of the correlation function of galaxies and clusters. A ready early studies have shown that on small scales the correlation function can be expressed as a power law (see [42]):

$$\xi(r) = (r/r_0)^{-1.8}; \quad (10)$$

where 1.8 is the power index, and $r_0 = 5 h^{-1} \text{ Mpc}$ is the correlation length. The correlation function of clusters of galaxies is similar, but shifted to larger scales, i.e. it has approximately the same power index but a larger correlation length, $r_0 = 25 h^{-1} \text{ Mpc}$. On small scales the correlation function reflects the fractal dimension, $D = 3$, of the distribution of galaxies and clusters [54]. On large scales the correlation function depends on the distribution of systems of galaxies.

In order to understand better how different geometries of the distribution of galaxies and clusters are reflected in the properties of the correlation function and power spectrum, we shall construct several mock samples with known geometrical properties, and calculate both functions. Here we use results of the study of geometrical properties of the correlation function [25,20].

The correlation function is determined by mutual distances of galaxies (or clusters) in real space, thus this function depends directly on the structure of galaxy systems themselves (on small separations which are comparable to

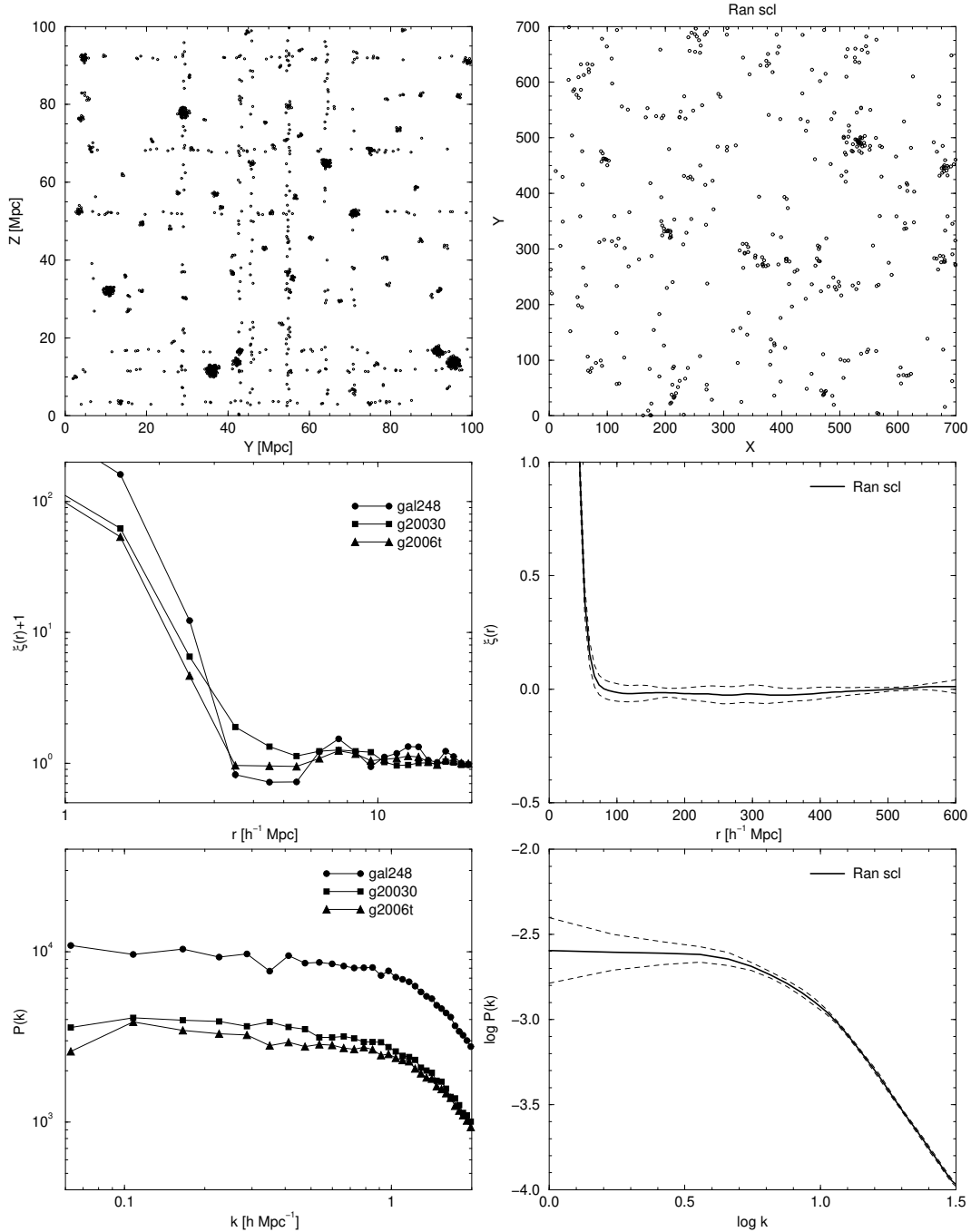


Fig. 4. The distribution of galaxies and clusters in random mock models (upper left and right panels, respectively), respective correlation functions (middle panels) and power spectra (lower panels). For explanations see text.

sizes of these systems), and on the distribution of galaxy systems (on separations which exceed the dimensions of galaxy systems). To see these effects separately we have constructed two series of mock samples. In the first series we change the distribution of galaxies on small scales following [25], in the second series we change the distribution of systems themselves [20]. In the first case we consider test particles as galaxies; they form two populations {

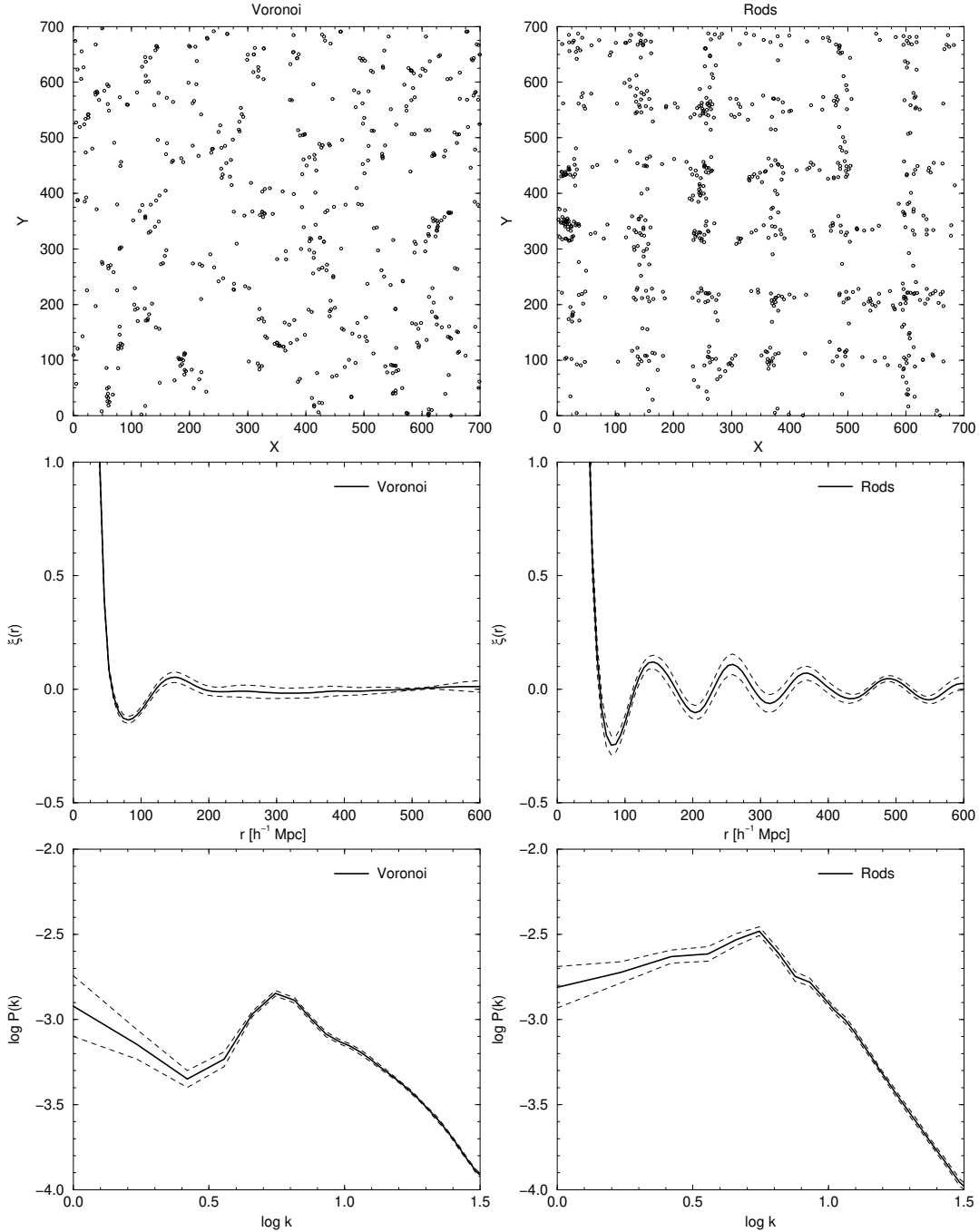


Fig. 5. The distribution of clusters in Voronoi and regular mock models (upper left and right panels, respectively), respective correlation functions (middle panels) and power spectra (lower panels). For explanations see text.

clusters and field galaxies. Clusters are located randomly in a cube of size $L = 100 h^{-1} \text{ Mpc}$; clusters have a varying number of member galaxies from 12 to 200, and an abundance and mass distribution in accordance with the observed cluster mass distribution (see the next subsection). Inside clusters galaxies are located randomly with an isothermal density distribution. For the field population we consider three cases. In the first model there is no

eld population at all; in Figure 4 this model is designated gal248 (it contains 248 clusters). The second model has 200 clusters and 6000 randomly located eld galaxies (designated as g2006t). The third model has also 200 clusters, but eld galaxies are located in filaments { each filament crosses one cluster in either x, y, or z{axis direction, randomly chosen, and has 30 galaxies; this sample is designated as g20030. The total number of galaxies in clusters and in the eld population in the two last models is approximately equal.

The distribution of galaxies in a sheet of thickness $15 h^{-1} \text{ Mpc}$ of the model g20030 is shown in the upper left panel of Figure 4. In the other two models the distribution of clusters is similar, but eld galaxies are distributed randomly or are absent. The correlation functions and power spectra of all three models are plotted in the middle and lower left panels, respectively. We see that the slope (power law index) of the correlation function at small separations is -3 in the pure cluster model, and -1.8 in other two models. These differences are due to the difference in the effective fractal dimension: $D = 3 - 0$ for the pure cluster model (clusters are spherically symmetrical); and $D = 1.2$ in a mixture of spherically symmetrical clusters and one-dimensional filaments. The power index depends on the partition of galaxies between the clustered and the eld populations. On scales of $r < 3 h^{-1} \text{ Mpc}$ the correlation function changes sharply. In the pure cluster model it has small negative values for $r > 3 h^{-1} \text{ Mpc}$, while in the random eld models $\xi(r) = 0$ for $r > 3 h^{-1} \text{ Mpc}$. In the model with filaments the correlation function is positive but has a smaller power index, of -1.2 . The change of the power index occurs on a scale equal to the diameter of clusters of galaxies. On larger scale the behaviour of the correlation function depends on properties of the eld population and on the distribution of clusters. In the absence of the eld there are only a few close neighbours of clusters, hence the slightly negative value of the correlation function; on larger scales the level of the correlation function reflects the distribution of clusters; clusters are distributed randomly and the level is approximately zero. In the random eld model galaxies are located also in the vicinity of clusters and the zero level of the correlation function begins immediately beyond the end of cluster galaxies. In the filamentary model the effective power index of the correlation function reflects the mean fractal dimension of filaments.

The power spectrum of all three models has a similar shape. On small scales the power index is negative and depends on the clustering law of galaxies in clusters. On larger scales the shape of the power spectrum depends on the distribution of galaxies and clusters on respective scales. Because both clusters and eld galaxies are essentially randomly distributed (the location of filaments is also random), the spectrum has a zero power index as expected for a random distribution. The amplitude of the power spectrum depends on the fraction of galaxies in clusters. In the pure cluster model the amplitude is much higher, and the difference in the amplitude depends on the fraction of

galaxies in clusters. This effect is similar to the influence of the void population discussed above.

Now we shall discuss models of the cluster distribution. We do not include the population of galaxies; instead we shall investigate how different distribution of clusters affects the correlation function and power spectrum. Here we assume that a fraction of clusters are located in superclusters, the rest form a field cluster population. We consider again three models: randomly distributed superclusters, regularly spaced superclusters, and superclusters formed by the Voronoi tessellation model. In the Voronoi model centers of voids are located randomly, and clusters are placed as far from void centres as possible. These models differ in their degree of regularity of the distribution of superclusters. The random supercluster model has no regularity and no built-in scale. The Voronoi model has a characteristic scale (the mean diameter of voids (determined by the number of voids in the sample volume)), but no regularity in the distribution of voids. In the regular model superclusters are located randomly along rods which form a regular rectangular grid of step size $120 h^{-1} \text{ Mpc}$; this scale defines the mean size of voids between superclusters, and also puts voids to a semi-regular honeycomb-like lattice. In addition a field population of isolated randomly located clusters is present in this model.

The distribution of clusters of the random, Voronoi, and regular model are shown in the upper panels of Figure 4 and 5; correlation functions are given in the middle panels, and power spectra in the lower panels. We see that on small scales all correlation functions are identical; power spectra on small wavenumbers are also identical. This is due to the fact that on these scales both functions are determined by the distribution of clusters within superclusters; and superclusters in all models were generated using the same algorithm as in generating galaxies in clusters. On larger scales there are important differences between models. In the random supercluster model the correlation function approaches zero at $r > 80 h^{-1} \text{ Mpc}$. In the Voronoi model it has a minimum around $r \approx 80 h^{-1} \text{ Mpc}$, followed by a secondary maximum at $r \approx 150 h^{-1} \text{ Mpc}$; thereafter it approaches zero. The correlation function of the regular rod model is oscillating: it has a series of regularly spaced maxima and minima with a period of $120 h^{-1} \text{ Mpc}$; the amplitude of oscillations decreases with increasing separation. The power spectrum of the random supercluster model is flat and featureless on large scales, while in the Voronoi and regular models it has a sharp maximum at wavenumber, which corresponds to the mean diameter of voids in models and to the period of oscillations of the correlation function. The shape of the power spectrum on large scales of these two models is, however, different.

These mock samples illustrate properties of the correlation function and power spectrum on small and large scales and their dependence on the distribution of galaxies and clusters within systems and on the distribution of systems

them selves. The correlation function of clusters of galaxies in rich superclusters is shown in the right panel of Figure 3. This function is oscillating with a period which corresponds to the maximum of the power spectrum at $k = 0.05 \text{ h Mpc}^{-1}$, seen in the left panel of the same Figure. We note that a periodicity of the distribution of high density regions with the same period has been observed in the direction of the galactic poles by Broadhurst et al. [8]. All these facts suggests that there exists a preferred scale of $130 \text{ h}^{-1} \text{ Mpc}$ in the Universe, and possibly also some regularity in the distribution of the supercluster(void network).

4.3 Mass function of clusters of galaxies

Masses of clusters of galaxies can be determined from the velocity dispersion of its member galaxies, or on the basis of their X-ray emission (using the hot gas as an indicator of the velocity dispersion in clusters), or else from the gravitational lens effect. Using masses of clusters and their abundance it is possible to calculate the number of clusters of different mass, $N(>M)$. This mass function is usually expressed in units of $h^{-1} M_0$ in a sphere of radius $1.5 \text{ h}^{-1} \text{ Mpc}$. The cluster mass function was derived by Bahcall & Cen [3], and also by Girardi et al. [27]. The function characterizes the distribution of systems of galaxies at the present epoch. There exist estimates of the abundance of clusters at high redshifts, but they are still very uncertain. The function $N(>M)$, and its specific value, $N(>10^{14} M_0)$, can be used to constrain cosmological parameters. We shall use this constraint in the next Section.

5 Cosmological parameters

As cosmological parameters we consider parameters which define the present and past structure of the Universe. Principal parameters are: the Hubble constant, which characterises the expansion speed of the Universe; the age and acceleration parameter of the Universe; densities of main constituents of the Universe: baryonic matter, dark matter and dark energy; and parameters, which define the amplitude and shape of the power spectrum of galaxies and matter. Cosmological parameters and descriptive functions can be used to test various scenarios of structure evolution.

The Hubble constant, h , can be estimated by several methods: through the ladder of various distance estimators from star clusters to cepheids in nearby galaxies, through the light curves of medium-distant supernovae, or using several physical methods (gravitational lensing, Sunyaev-Zeldovich effect). Summaries of recent determinations are given in [41,47]. A mean value of recent

determinations is $h = 0.65 \pm 0.07$.

The baryon density can be determined most accurately from observations of the deuterium, helium and lithium abundances in combination with the nucleosynthesis constraints. The best available result is $\Omega_b h^2 = 0.019 \pm 0.002$ [11].

The total density of matter, $\Omega_{tot} = \Omega_m + \Omega_v$, determines the position of the first Doppler peak of the angular spectrum of CMB temperature fluctuations; here Ω_m and Ω_v are the densities of matter and dark (vacuum) energy, respectively. Recent observations show that the maximum of the first Doppler peak lies at $l \approx 200$ [17,30]. This indicates that $\Omega_{tot} \approx 1$. Since this is the theoretically preferred value, I assume in the following that $\Omega_{tot} = 1$.

There exist a number of methods to estimate the density of matter, $\Omega_m = \Omega_b + \Omega_c + \Omega_n$, where Ω_b , Ω_c , and Ω_n are the densities of baryonic matter, cold dark matter (CDM), and hot dark matter (HDM), respectively. The luminosity (distance) method, used in the distant supernova project, yields $\Omega_m = 0.28 \pm 0.05$ [43,45]. Another method is based on X-ray data on clusters of galaxies, which gives the fraction of gas in clusters, $f_{gas} = \Omega_b / \Omega_m$. If compared to the density of the baryonic matter one gets the estimate of the total density, $\Omega_m = 0.31 \pm 0.05$ ($h=0.65$)¹⁼³ [39]. A third method is based on the geometry of the Universe. Observations show the presence of a dominant scale, $l_0 = 130 \pm 10 h^{-1}$ Mpc, in the distribution of high-density regions [8,21,20]. A similar phenomenon is observed in the distribution of Lyman-break galaxies [9] at high redshift, $z \approx 3$. We can assume that this scale is primordial and comoves with the expansion; in other words { it can be used as a standard ruler. The relation between redshift difference and linear comoving separation depends on the density parameter of the Universe; for a closed universe one gets a density estimate $\Omega_m = 0.4 \pm 0.1$. The same method was applied for the distribution of quasars by Roukema & Mamon [46] with the result $\Omega_m = 0.3 \pm 0.1$. Finally, the evolution of the cluster abundance with time also depends on the density parameter (see [4] for a review). This method yields an estimate $\Omega_m = 0.4 \pm 0.1$ for the matter density. The formal weighted mean of these independent estimates is $\Omega_m = 0.32 \pm 0.03$.

Cosmological parameters enter as arguments in a number of functions which can be determined from observations. These functions include the power spectrum of galaxies, the angular spectrum of temperature fluctuations of the CMB radiation, the cluster mass and velocity distributions. I accept the power spectrum of galaxies according to a summary in [22] with the addition of the recent determination of the cluster power spectrum [38]. The amplitude of the power spectrum can be expressed through the δ_8 parameter { rms density fluctuations within a sphere of radius $8 h^{-1}$ Mpc. This parameter was determined for the present epoch for galaxies, $(\delta_8)_{gal} = 0.89 \pm 0.09$ [22]. For the CMB angular

spectrum I use recent BOOMERANG and MAXIMA I measurements [17,30]. For the cluster mass distribution I use the determinations by [3] and [27].

6 Cosmological models

The power spectra of matter and the angular spectra of CMB can be calculated for a set of cosmological parameters using the CMBFAST algorithm [50]; spectra are COBE normalized. The cluster abundance and mass distribution functions can be calculated by the Press-Schechter [44] algorithm. We have used these algorithms to test how well cosmological parameters are in agreement with these descriptive functions.

One problem in comparing cosmological models with observations is related to the fact that from observations we can determine the power spectra and correlation functions of galaxies and clusters of galaxies, but using models we can do that for the whole matter. Power spectra of galaxies and matter are related through the bias parameter. There exist various methods to estimate the bias parameter, using velocity data. Here we use another method which is based on the numerical simulation of the evolution of the Universe. During dynamical evolution matter flows away from low-density regions and forms filaments and clusters of galaxies. This flow depends slightly on the density parameter of the model. The fraction of matter in the clustered population can be found by counting particles with local density values exceeding a certain threshold. To separate void particles from clustered particles we have used the mean density, since this density value divides regions of different cosmological evolution, see eq. (1). Hydrodynamical simulations by Cen & Ostriker [12] confirmed that galaxy formation occurs only in overdense regions.

We express the epoch of simulations through the δ_8 parameter, which was calculated by integrating the power spectrum of matter. It is related to the observed value of $(\delta_8)_{gal}$ by the equation (compare with eq. (5, 6))

$$(\delta_8)_{gal} = b_{gal}(\delta_8)_m ; \quad (11)$$

here we assume that $b_{gal} = b_c$. This equation, and the observed value of $(\delta_8)_{gal}$, yields one equation between $(\delta_8)_m$ and b_c (or F_{gal}); it is shown in the upper left panel of Figure 6 by a bold line with error corridor. The other equation is given by the growth of F_{gal} with epoch. For two LCDM models with density parameter $\Omega_m = 0.4$ the growth of F_{gal} is shown by dashed curves in the upper left panel of Figure 6 [23]. By simultaneous solution of both equations we found all three quantities of interest for the present epoch: rms density fluctuations of matter $(\delta_8)_m = 0.64 \pm 0.06$, the fraction of matter in the clustered population, $F_{gal} = 0.70 \pm 0.09$, and the biasing parameter $b_{gal} = 1.4 \pm 0.1$.

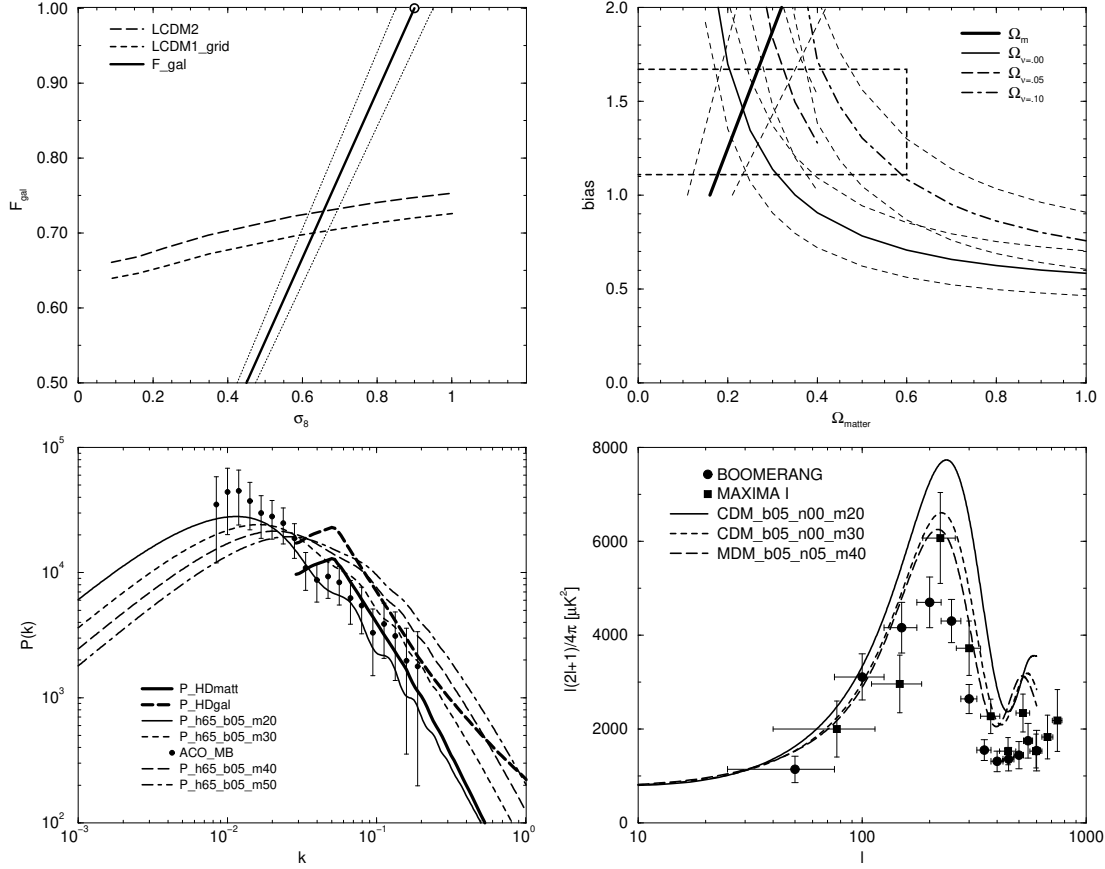


Fig. 6. Upper left: the fraction of matter in the clustered population associated with galaxies as a function of σ_8 for 2 LCDM models (dashed curves); and the relation between F_{gal} and $(\sigma_8)_m$ (bold solid line). Upper right: the biasing parameter needed to bring the amplitude σ_8 of the model into agreement with the observed σ_8 for galaxies and for LCDM and MDM models with various matter density Ω_m and HDM density, Ω_b . The dashed box shows the range of the bias parameter allowed by numerical simulations of the evacuation of voids. Lower left: power spectra of LCDM models with various Ω_m . Lower right: angular spectra of CMB for LCDM and MDM models for various Ω_m .

The CMBFAST algorithm yields for every set of cosmological parameters the σ_8 value for matter. It is calculated using the linear growth model of density perturbations. From observations we know this parameter for galaxies, $(\sigma_8)_{gal}$. Using eq. (11) we can calculate the biasing parameter b_{gal} , needed to bring the theoretical power spectrum of matter into agreement with the observed power spectrum of galaxies. This parameter must lie in the range allowed by numerical simulations of the evolution of structure. Results of calculations for a range of Ω_m are shown in the upper right panel of Figure 6, using the Hubble constant $h = 0.65$, baryon density $\Omega_b = 0.05$, and HDM densities $\Omega_b = 0.00; 0.05; 0.10$. The biasing parameter range shown in the Figure is larger than expected from calculations described above; this range corresponds to the maximum allowed range of the fraction of matter in the clustered population expected from analytic estimates of the speed of void evacuation.

Power spectra for LCDM models ($\Omega_m = 0.2$ to 0.5) are shown in the lower left panel of Figure 6. We see that with increasing Ω_m the amplitude of the power spectrum on small scales (and respective σ_8 values) increases, so that for high Ω_m the amplitude of the matter power spectrum exceeds the amplitude of the galaxy power spectrum. This leads to bias parameter values $b < 1$. Such values are unlikely since the presence of matter in voids always increases the amplitude of the galaxy power spectrum relative to the matter spectrum. If other constraints demand a higher matter density value, then the amplitude of the matter power spectrum can be lowered by adding some amount of HDM. However, supernova and cluster X-ray data exclude density values higher than $\Omega_m = 0.4$; thus the possible amount of HDM is limited. The lower right panel of the Figure 6 shows the angular spectrum of temperature anisotropies of CMB for different values of the density parameter Ω_m . We see that a low amplitude of the first Doppler peak of the CMB spectrum prefers a higher Ω_m value: for small density values the amplitude is too high. So a certain compromise is needed to satisfy all data.

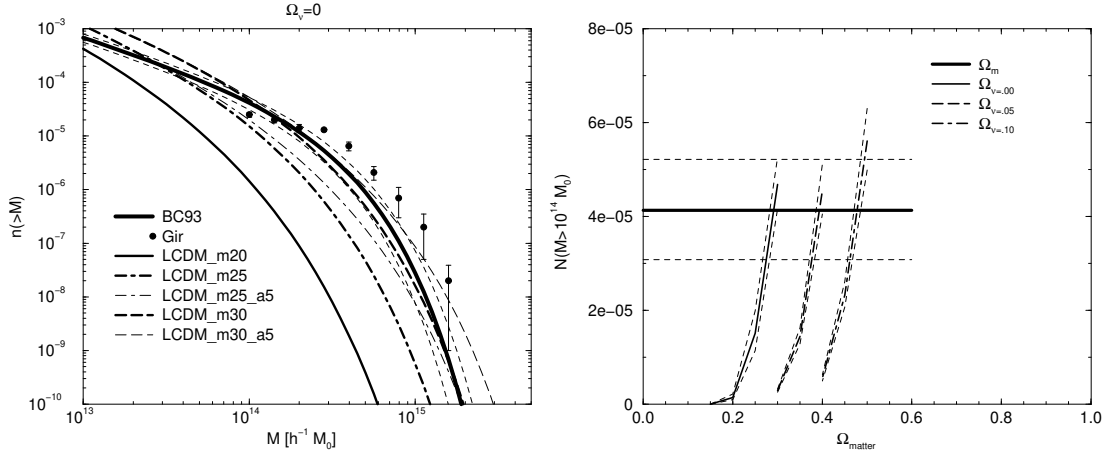


Fig. 7. Left: cluster mass distribution for LCDM models of various density Ω_m , with and without a Chung bump of amplitude $a = 0.5$. Right: cluster abundance of LCDM and MDM models of various density of matter Ω_m and hot dark matter Ω_h .

The cluster mass distribution for LCDM models $0.2 < \Omega_m < 0.3$ is shown in the left panel of Figure 7. We see that low-density models have a too low abundance of clusters over the whole range of cluster masses. The best agreement with the observed cluster abundance is obtained for a LCDM model with $\Omega_m = 0.3$, in good agreement with direct data on matter density. In this Figure we show also the effect of a bump in the power spectrum, which is seen in the observed power spectrum of galaxies and clusters [22]. Several modifications of the inflation scenario predict the formation of a break or bump in the power spectrum. The influence of the break suggested by Lesgourgues, Polarski and Starobinsky [32] was studied by Gramann and Hutsi [28]. Another mechanism was suggested by Chung et al. [13]. To investigate the latter case we have used a value of $k_0 = 0.04 \text{ h Mpc}^{-1}$ for the long wavelength end of the bump, and $a = 0.3$ to 0.8 for the amplitude parameter. Our results show that

such a bump only increases the abundance of very massive clusters. In the right panel of Figure 7 we show the cluster abundance constraint for clusters of masses exceeding 10^{14} solar masses; the curves are calculated for LCDM and MDM models with $n_s = 0.00; 0.05; 0.10$. We see that the cluster abundance criterion constrains the matter and HDM densities in a rather narrow range.

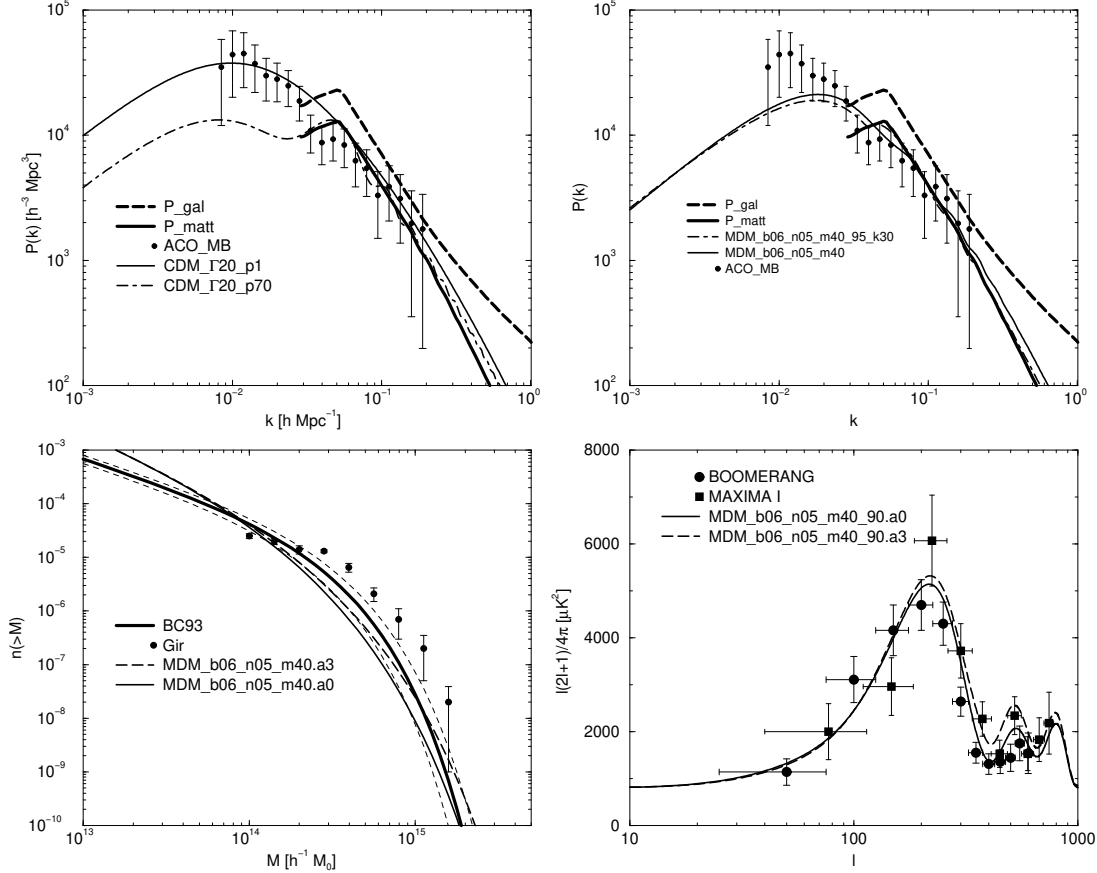


Fig. 8. Upper left: power spectra of a LCDM model with and without Starobinsky modification. Upper right: power spectra of MDM models with and without Chung modification. Lower left: cluster mass distributions for MDM models with and without Chung modification. Lower right: angular power spectra of tilted MDM models with and without Chung modification (amplitude parameter $a = 0.3$).

The power spectra of LCDM models with and without the Starobinsky break are shown in the upper left panel of Figure 8; these models were calculated for the parameter $n_s = n_m h = 0.20$. In the case of the spectrum with a bump we have used MDM models as a reference due to the need to decrease the amplitude of the spectrum on small scales; these spectra are shown in the upper right panel of Figure 8. Power spectra are compared with the observed galaxy power spectrum [22] and with the new cluster power spectrum [38], reduced to the amplitude of the galaxy power spectrum. Also the matter power spectrum is shown, for which we have used a biasing factor $b_c = 1.3$ [23]. We see that the Starobinsky model reproduces well the matter power spectrum on small and intermediate scales, but not the new data by Miller & Batuksi. The

modification by Chung et al. [13] with amplitude parameter $a = 0.3$ fits well all observational data. The cluster mass distribution for the Chung model is shown in the lower left panel of Figure 8, and the angular spectrum of CMB temperature fluctuations in the lower right panel of Figure 8. In order to fit simultaneously the galaxy power spectrum and the CMB angular spectrum we have used a tilted MDM model with parameters $n = 0.90$, $b = 0.06$, $\alpha_n = 0.05$, and $\alpha_m = 0.4$.

BOOMERANG and MAXIMA I data have been used in a number of studies to determine cosmological parameters [7,17,30,56,59]. In general, the agreement between various determinations is good; however, some parameters differ. There is a general trend to interpret new CMB data in terms of a baryon fraction higher than expected from the nucleosynthesis constraint; $h^2 \Omega_b = 0.03$. Tegmark & Zaldarriaga [56] suggested a relatively high matter density, $h^2 \Omega_m = 0.33$. On the other hand, velocity data suggest a relatively high amplitude of the power spectrum, $\Omega_m^{0.6} = 0.54$, which in combination with distant supernova data yields $\Omega_m = 0.28 - 0.10$, and $\Omega_b = 1.17 - 0.2$ [7].

Our analysis has shown that a high value of the density of matter, $\Omega_m > 0.4$, is difficult to reconcile with current data on supernova and cluster abundances. Similarly, a high amplitude of the matter power spectrum, $\Omega_b > 1$, seems fairly incompatible with the observed amplitude of the galaxy power spectrum and reasonable bias limits. This conflict can be avoided using a tilted initial power spectrum, and a MDM model with a moderate fraction of HDM, as discussed above. The best models suggested so far have $0.3 < \Omega_m < 0.4$, $0.90 < n < 0.95$, $0.60 < h < 0.70$, $\alpha_n < 0.05$. Matter density values lower than 0.3 are strongly disfavoured by the cluster abundance constraint, and values higher than 0.4 by all existing matter density estimates. This upper limit of the matter density, in combination with the cluster abundance and the amplitude of the power spectrum, yields an upper limit to the density of hot dark matter. We can consider this range of cosmological parameters as a set which fits well all constraints. This set of cosmological parameters is surprisingly close to the set suggested by Ostriker & Steinhardt [40]. Now it is supported by much more accurate observational data.

Acknowledgements

I thank M. Einasto, M. Gramann, V. Müller, A. Starobinsky, E. Saar and E. Tago for fruitful collaboration and permission to use our joint results in this review, and H. Andemach for suggestions to improve the text. This study was supported by the Estonian Science Foundation grant 2625.

References

- [1] Abell, G. O. 1958, *Astrophys. J. Suppl.*, 3, 211
- [2] Abell, G. O., Corwin, H. G. & Lowin, R. P. 1989, *Astrophys. J. Suppl.*, 70, 1
- [3] Bahcall, N. A., & Cen, R. 1993, *Astrophys. J.*, 407, L49
- [4] Bahcall, N. A., Ostriker, J. P., Perlmutter, S., & Steinhardt, P. J., 1999, *Science*, 284, 1482, astro-ph/9906463
- [5] Blumenthal, G. R., Faber, S. M., Primack, J. R. & Rees, M. J. 1984, *Nature*, 311, 517
- [6] Bond, J. R., Kofman, L. & Pogosyan, D. 1996, *Nature*, 380, 603
- [7] Bridle, S. L., Zehavi, I., Dekel, A., Lahav, O., Hobson, M. P., & Lasenby, A. N., 2000, *Mon. Not. R. astr. Soc.* (in press), astro-ph/0006170
- [8] Broadhurst, T. J., Ellis, R. S., Koop, D. C., & Szalay, A. S., 1990, *Nature*, 343, 726
- [9] Broadhurst, T. J., & Jaes, A. H., 2000, *Astrophys. J.* (in press), astro-ph/9904348
- [10] Bunn, E. F., & White, M. 1997, *Astrophys. J.*, 480, 6
- [11] Burles, S., Nollett, K. M., Truran, J. N., & Tumer, M. S., 1999, *Phys. Rev. Lett.*, 82, 4176
- [12] Cen, R., & Ostriker, J. P. 1992, *Astrophys. J.*, 399, L113
- [13] Chung, D. J. H., Kolb, E. W., Riotto, A., & Tkachev, I. I., 1999, hep-ph/9910437
- [14] da Costa, L. N., 1999, in *Evolution of Large Scale Structure: from Recombination to Garching*, T. Banday & R. Sheth eds., Enschede: PrintPartners, p. 87, astro-ph/9812258
- [15] Dalton, G. B., Maddox, S. J., Sutherland, W. J., & Efsthathiou, G. 1997, *Mon. Not. R. astr. Soc.*, 289, 263
- [16] Davis, M. & Peebles, P. J. E. 1983, *Astrophys. J.*, 267, 465
- [17] de Bernardis, P. et al., 2000, *Nature*, 404, 955
- [18] de Vaucouleurs, G., de Vaucouleurs, A. & Corwin, H. G. 1976, *Second Reference Catalog of Bright Galaxies*, Austin: Univ. Texas Press
- [19] Efsthathiou, G., Sutherland, W. J., & Maddox, S. J., 1990, *Nature*, 348, 705
- [20] Einasto, J., Einasto, M., Frisch, P., Gottlober, S., Muller, V., Saar, V., Starobinsky, A. A., & Tucker, D., 1997b, *Mon. Not. R. astr. Soc.*, 289, 813
- [21] Einasto, J., Einasto, M., Gottlober, S., Muller, V., Saar, V., Starobinsky, A. A., Tago, E., Tucker, D., Andemach, H., & Frisch, P., 1997a, *Nature*, 385, 139

- [22] Einasto, J., Einasto, M., Tago, E., Starobinsky, A. A., Atrio-Barandela, F., Muller, V., Knebe, A., Frisch, P., Cen, R., Andemach, H., & Tucker, D., 1999a, *Astrophys. J.*, 519, 441
- [23] Einasto, J., Einasto, M., Tago, E., Muller, V., Knebe, A., Cen, R., Starobinsky, A. A. & Atrio-Barandela, F., 1999b, *Astrophys. J.*, 519, 456
- [24] Einasto, J., Joeveer, M. & Saar, E. 1980, *Mon. Not. R. astr. Soc.*, 193, 353
- [25] Einasto, M. 1991, *Mon. Not. R. astr. Soc.*, 252, 261
- [26] Einasto, M., Tago, E., Jaaniste, J., Einasto, J., & Andemach, H., 1997c, *Astron. & Astrophys. Suppl.*, 123 119
- [27] Girardi, M., Borgani, S., Guricín, G., Mardirossian F., & Muzzetti, M., 1998, *Astrophys. J.*, 506, 45
- [28] Gramann, M., & Hutshi, G., 2000, *Mon. Not. R. astr. Soc.* 316, 631, *astro-ph/0003455*
- [29] Guzzo, L., 1999, *astro-ph/9911115*
- [30] Hanany, S., et al., 2000, *Astrophys. J.* (in press), *astro-ph/0005123*
- [31] Joeveer, M. & Einasto, J. 1978, *The Large Scale Structure of the Universe*, eds. M. S. Longair & J. Einasto, Dordrecht: Reidel, p. 241
- [32] Lesgourgues, J., Polarski, D., & Starobinsky, A. A., 1998, *Mon. Not. R. astr. Soc.*, 297, 769, *astro-ph/9711139*
- [33] Longair, M. S., & Einasto, J., eds., 1978, *The Large Scale Structure of the Universe*, Dordrecht: Reidel
- [34] Loveday, J., 1999, in *Second International Workshop on Dark Matter in Astro and Particle Physics*, eds. H. V. Klapdor-Kleingrothaus & L. Baudis, Bristol & Philadelphia: Inst. of Physics Publ., p. 305, *astro-ph/9810130*
- [35] Maddox, S., 1998, *Large Scale Structure: Tracks and Traces*, eds. V. Muller, S. Gottlobber, J. P. Muckel & J. Wambsganss, Singapore: World Scientific, p. 91
- [36] Maddox, S. J., Efstathiou, G., & Sutherland, W. J. 1990, *Mon. Not. R. astr. Soc.*, 246, 433
- [37] Maddox, S. J., Efstathiou, G., & Sutherland, W. J. 1996, *Mon. Not. R. astr. Soc.*, 283, 1227
- [38] Miller, C. J. & Batuski D. J., 2000, *Astrophys. J.* (in press), *astro-ph/0002295*
- [39] Mohr, J. J., Reese, E. D., Ellington, E., Lewis, A. D., & Evrard, A. E., 2000, *Astrophys. J.* (in press), *astro-ph/0004242*
- [40] Ostriker, J. P., & Steinhardt, P. J., 1995, *Nature*, 377, 600
- [41] Parodi, B. R., Saha, A., Sandage, A., & Tamman, G. A., 2000, *Astrophys. J.* 540, 634, *astro-ph/0004063*

- [42] Peebles, P.J.E. 1980, *The Large Scale Structure of the Universe*, Princeton: Princeton University Press
- [43] Perlmutter, S., et al. 1998, *Astrophys. J.*, 517, 565
- [44] Press, W.H., & Schechter, P.L., 1974, *Astrophys. J.*, 187, 425
- [45] Riess, A.G., et al. 1998, *Astron. J.*, 116, 1009
- [46] Roukema, B.F., & Mamon, G.A., 2000, *Astron. Astrophys.*, 358, 395, astro-ph/9911413
- [47] Sakai, S., et al. 2000, *Astrophys. J.* 529, 698, astro-ph/9909269
- [48] Sandage, A. & Tammann, G.A. 1981, *A Revised Shapley-Ames Catalog of Bright Galaxies*, Washington: Carnegie Inst. Washington
- [49] Seldner, M., Siebers, B., Groth, E.J. & Peebles, P.J.E. 1977, *Astron. J.*, 82, 249
- [50] Seljak, U., & Zaldarriaga, M., 1996, *Astrophys. J.*, 469, 437
- [51] Shane, C.D. & Vartanen, C.A. 1967, *Publ. Lick Obs.* 22
- [52] Shectman, S.A., Landy, S.D., Oemler, A., Tucker, D.L., Lin, H., Kirshner, R.P., Schechter, P.L., 1996, *Astrophys. J.*, 470, 172
- [53] Shapley, H. & Ames, A. 1932, *Harvard Ann.* 88, Part II
- [54] Szalay, A.A., & Schramm, D.M., 1985, *Nature*, 314, 718
- [55] Tarenghi, M., Tit, W.G., Chincarini, G., Rood, H.J. & Thompson, L.A. 1978, *The Large Scale Structure of the Universe*, eds. M.S. Longair & J. Einasto, Dordrecht: Reidel, p. 263
- [56] Tegmark, M., & Zaldarriaga, M., 2000, astro-ph/0004393
- [57] Tit, W.G. & Gregory, S.A. 1978, *The Large Scale Structure of the Universe*, eds. M.S. Longair & J. Einasto, Dordrecht: Reidel, p. 267
- [58] Tully, R.B. & Fisher, J.R. 1978, *The Large Scale Structure of the Universe*, eds. M.S. Longair & J. Einasto, Dordrecht: Reidel, p. 214
- [59] White, M., Scott, D., & Pierpaoli, E., 2000, astro-ph/0004385
- [60] Zeldovich, Ya.B., 1970, *Astron. Astrophys.*, 5, 84
- [61] Zeldovich, Ya.B., 1978, *The Large Scale Structure of the Universe*, eds. M.S. Longair & J. Einasto, Dordrecht: Reidel, p. 409
- [62] Zeldovich, Ya.B., Einasto, J. & Shandarin, S.F. 1982, *Nature*, 300, 407
- [63] Zwicky, F., Field, P., Herzog, E., Kapowicz M. & Kowal, C.T. 1961{68, *Catalogue of Galaxies and Clusters of Galaxies*, 6 volumes. Pasadena, California Inst. Techn.